

Numerical Investigation of Vortex Shedding and Flow Around a Smooth Circular Cylinder in Upper Transition Regime by Using URANS

M.I.Khan¹, S.A.Masood²

^{1,2}International Islamic University, Islamabad, Pakistan

¹muhammad.ishfaq@iiu.edu.pk

Abstract- Flow around a circular cylinder is of prime interest of many researchers. In this research flow around a smooth circular cylinder has been explored in Upper Transition Regime (1.5×10^6 - 4×10^6) at Re 1.5×10^6 , 2×10^6 , 2.7×10^6 , 3×10^6 and 3.6×10^6 by employing Two Dimensional Unsteady Reynolds Averaged Navier-Stokes Equations (2D URANS) SST k- ω model. The objective of the research is to find out the viability of the model in the regime from engineering point of view. The results are compared with sparsely published experimental and numerical data for the regime. Based on the comparison it is concluded that the model predicts satisfactory results, from engineering point of view, for the regime where turbulence is anisotropic.

Keywords- Numerical Models, Turbulent Flow, Smooth Circular Cylinder, Upper Transition Regime .

I. INTRODUCTION

Flow around a circular cylinder is a classical problem of fluid mechanics. The problem is representation of many engineering applications like landing gear, marine structures like risers and bridge columns, high-rise chimneys, towers etc. Some of these applications operate at Reynolds Numbers (Re = UD/v) that are in upper transition regime (1.5×10^6 - 4×10^6). Re is based on the free stream velocity (U), diameter of cylinder (D) and kinematic viscosity (v). A scarce amount of both experimental and numerical investigations are available in literature for the upper transition regime (UTR) and Tran-Critical Regime (TCR) because:

- i) it is difficult and very expensive to achieve such high Re in the experimental set up,
- ii) very few engineering applications operate in the said regimes e.g. bridge columns during floods, landing gear of an airplane, and
- iii) presence of strong turbulence anisotropy in the regime.

Both experimental and numerical data regarding UTR

reported in literature is only at discrete values of Re i.e., 1.5×10^6 , 2×10^6 , 3×10^6 and 3.6×10^6 .

Most of the data reported in literature focuses on Sub-critical (300 - 3×10^5), Critical/ Lower Transition, (3×10^5 - 3.5×10^5), Super-Critical (3.5×10^5 - 1.5×10^6) since most of the engineering applications operate in these regimes, and presence of phenomenon of drag crisis and lower magnitudes of anisotropic turbulence. The research on these regimes is multifaceted and diverse. Hongi Jiang worked on separation angle of the flow past cylinder at Re 190-270 and concluded that the prediction of the separation angle plays a vital role on the wake behind cylinder. [1] M.S. Aswathy et. al. worked on nonlinear effect of presence of stochastic noise on nonlinear dynamics of vortex induced vibrations (VIV) of a circular cylinder at Re 5×10^3 to 4×10^4 . They concluded that the uncertainty in the noise acting on the cylinder has a significant impact on the negative aerodynamic damping, altering the frequency characteristics. [2] Desai et. al. in their experimental investigation at Re $1.49 \times 10^5 \leq Re \leq 5 \times 10^5$ concluded that a two stage drag crisis happens in the regime with specific variations in trends of coefficients of drag and coefficients of lifts. [3] Moreau et. al. in their numerical investigation at Re 2.43×10^5 concluded that vortex shedding is the major source of noise in the flow across a circular cylinder. [4] It becomes clear from this brief insight into literature that though the research is multifaceted, yet it is dedicated to lower flow regimes to date.

Experimental investigations are time consuming, labor intensive and costly. On one side, these investigations provide a lesser control over parameters and a limited insight. Researchers now a days prefer to conduct numerical investigations and try to benchmark their results with experimental data reported by earlier researchers of the field. [5] On the other hand, numerical investigations have their own limitations i.e. computational power and storage memory. Researchers from industry opt for 2D URANS over 3D URANS, Large Eddy Simulation (LES) and Direct Numerical Simulation (DNS), because of their

capacity to deliver a valuable insight and satisfactory bench marked results with considerably low computational power and storage memory. [6] LES and DNS have been employed by researchers for low Re and not high Re; because of high demand of computational resources due to involvement associated high level of anisotropic turbulence at higher Re. The most common Re for which LES and/or DNS are 3900, 5500, 2×10^4 , $2-4 \times 10^4$ and $2-8.5 \times 10^5$. [7-9]

As mentioned earlier, a scarce amount of data is available for UTR at discrete Re. Most of these reported results are achieved from k-ε based models of 2D URANS. Shaghfian et. al. (2003) employed 2D RANS Craft–Launder–Suga k-ε model at Re 3.6×10^6 of UTR. They reported that coefficient of drag (Cd) to be 0.64 & 0.67 for using linear terms, quadratic and terms (excluding c6 & c7), respectively. Their results exhibited a decreasing trend in contrast to the experimental trends reported by Roshko (1960) and Achenbach(1968). [10, 11] They also reported the inability of the models to predict attached separation bubble. [12]. A.C. Benim et. al. (2007) explored UTR by employing k-ε with wall function and STT models of RANS. Their reported results do not depict accuracy in terms of both quality and quantity in UTR. [13] M.C. Ong et. al. (2008), applied k-ε model at Re 1×10^6 , 2×10^6 and 3.6×10^6 . The values of coefficient of Cd reported by them were though closer to the reported experimental results of Catalano et. al., however they clearly lacked both quality and quantity with respect to most of the reported experimental data. [14] B.N. Rajani et. al. (2012) employed URANS k-ε Model, SST, S-A Model and k-ε- v^2-f at Re 10^5 , 8.5×10^5 , 3.6×10^6 and 10^7 . They observed that the models were unable to capture the trends of Cd despite a reasonable temporal and spatial resolution. [15] Mehmet Ishak Yuce (2016) employed SST-K-ω model in RANS at Re 1.5×10^6 , 2×10^6 and Re 4×10^6 . Their reported Cd was under predicted and results did not follow the trend reported in experiments as well. [16]

The research conducted so far in upper transition ($1.5 \times 10^6-4 \times 10^6$) employs 2D RANS due to its advantages over LES and DNS in terms of good balance between of computational resources (processing power and storage memory) and accuracy. [6] The research reported in literature so far for UTR uses k-ε and its variants models at Re 2×10^6 , 3×10^6 , 3.6×10^6 and 4×10^6 , except Ishak Yuce et. al., who employed 2D RANS SST-K-ω model at Re 1.5×10^6 , 2×10^6 and 4×10^6 . The reported results are reasonably accurate from engineering point of view in terms of Cd and lack in capturing the attached separation bubble as found by Shaghfian et. al.

The objective of this research is to find out suitability of 2D URANS SST-K-ω model for engineering applications in UTR in terms of predicting accurate values of Cd and attached separation bubble at Re

1.5×10^6 , 2×10^6 , 2.7×10^6 , 3×10^6 and 3.6×10^6 . The results will be compared with experimental results of Achenbach and the numerical investigations of Shaghfian et. al. and Ishak Yuce et. al. [10, 12, 16]

II. MATHEMATICAL MODEL

A. Governing Equations:

Decomposed conservation of mass and momentum equations of Reynolds Averaged Navier-Stokes Equations for unsteady compressible flow are:

Continuity:

$$\frac{\partial \bar{\rho}}{\partial t} + \frac{\partial}{\partial x_i} (\bar{\rho} \tilde{u}_i) = 0 \quad (1)$$

Momentum:

$$\frac{\partial}{\partial t} (\bar{\rho} \tilde{u}_i) + \frac{\partial}{\partial x_j} (\bar{\rho} \tilde{u}_i \tilde{u}_j) = - \frac{\partial \bar{p}}{\partial x_i} + \frac{\partial}{\partial x_j} (\tilde{\sigma}_{i,j} - \overline{\rho u_j'' u_i''}) \quad (2)$$

Boussinesq modelled the Reynolds Stresses as:

$$-\overline{\rho u_j'' u_i''} = \mu_t \left(\frac{\partial u_i}{\partial x_j} + \frac{\partial u_j}{\partial x_i} \right) \quad (3)$$

B. Turbulent Model

Turbulence Kinetic Energy:

$$\frac{\partial k}{\partial t} + U_j \frac{\partial k}{\partial x_j} = P_k - \beta^* k \omega + \frac{\partial}{\partial x_j} \left[(v + \sigma_k v_T) \frac{\partial k}{\partial x_j} \right] \quad (4)$$

Specific Dissipation Rate:

$$\frac{\partial \omega}{\partial t} + U_j \frac{\partial \omega}{\partial x_j} = \alpha S^2 - \beta \omega^2 + \frac{\partial}{\partial x_j} \left[(v + \sigma_\omega v_T) \frac{\partial \omega}{\partial x_j} \right] + 2(1 - F_1) \sigma_{\omega 2} \frac{1}{\omega} \frac{\partial k}{\partial x_i} \frac{\partial \omega}{\partial x_i} \quad (5)$$

Revised model constants are: [17]

σ_k	$\sigma_{\omega,1}$	$\sigma_{\omega,2}$	γ_2	β_2	β^*
= 1.0	= 2.0	= 1.17	= 0.44	= 0.083	= 0.09

III. FLOW DOMAIN AND BOUNDARY CONDITIONS

Circular cylinder of diameter (d) 0.4m is placed in fluid domain. Inlet is at 8 m (20xd) upstream, outlet is at 20m (50xd) downstream and side walls are 6m (15xd) away from the center of the cylinder. The schematics of the domain is given in Fig. 1.

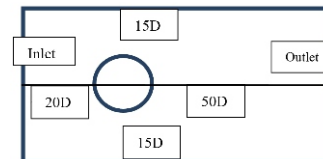


Fig. 1: Fluid Domain and Circular Cylinder Position

The free air stream velocities in x-direction at the inlet for Re 1.5×10^6 , 2×10^6 , 2.7×10^6 , 3×10^6 and 3.6×10^6 used for the numerical investigation are given the Table 1.

Table. 1 Velocity and Reynolds Numbers used in the research

Sr. No.	Velocity (m/s)	Re (10^6)
1	131.437	3.6
2	109.530	3
3	100	2.7
4	73.0204	2
5	54.765	1.5

Pressure at outlet was set 0 Pa and 0 specific shear is invoked for side walls. No slip boundary condition is opted for the cylinder.

IV. COMPUTATIONAL DOMAIN AND BOUNDARY LAYER TREATMENT

Structure mesh is constructed with concentric circles of radii 0.201m, 0.6 m, 0.8 m, 1.2 m, 2.4 m, 3.2 m and 4.8 m around the cylinder. The remaining domain is divided in equal parts to accommodate a structured mesh. Inflation boundary layer is employed with smooth transition having first layer height of less than 3.6×10^{-6} m; calculated by setting $y^+ = 1$, as per equations (6), (7), (8) and (9).

$$C_f = [2 \log_{10}(Re_x) - 0.65]^{-2.3} \quad \text{for } Re_x < 10^9 \quad (6)$$

$$\tau_w = C_f \frac{1}{2} \rho U_{free\ stream}^2 \quad (7)$$

$$u_* = \sqrt{\frac{\tau_w}{\rho}} \quad (8)$$

$$y = \frac{\mu y^+}{\rho u_*} \quad (9)$$

Where:[18]

y is absolute distance from wall,
 C_f is co-efficient of skin friction,
 τ_w is wall shear stress,
 u_* is friction velocity.

V. NUMERICAL SCHEME

Density based solver was selected to accommodate chances of variation of density at high local speed of fluid for the leading side of the cylinder. Transient time is selected to get ensemble averaged RANS with respect to time. Since, wake and flow around a circular cylinder in UTR is highly turbulent and is subjected to varying length and time scales, therefore implicit numerical scheme was opted. The

implicit scheme also has less stringent stability requirements than explicit. Roe flux-difference splitting (Roe-FDS) was employed to model convective flux, because there was no discontinuities/shock waves expected in the flow.

Green-Gause node based spatial discretization was used to maintain second order accuracy of discretization in determining the gradients from the surrounding cells. Cell to face spatial discretization limiter has been used. Pressure and momentum equations was discretized using second order upwind scheme to achieve higher accuracy at cell faces. Turbulent kinetic energy and specific dissipation rates was also discretized using first order upwind schemes to ensure stability of the solution. Transient first order implicit formulation was employed to ensure a stable solution as the second order implicit formulation may prone to become unstable at high Re .

Relaxation factor plays a vital role in stability of solution by removing steep oscillations to dampen the numerical process. Relaxation factor of 0.75 has been invoked to achieve the best possible numerical damping in case of any instability.

The numerical discretization and preprocessing leads to a system of equations that need to be solved in matrix form. The resulting matrices are often huge and involve different scales of solution. These scales are exploited to solve huge matrices by adopting Algebraic Multi Grid (AMG) solver technique which not only speeds up the solution process but also limits the high frequency errors by employing Gause-Siedel Smoother for scalar parameters.

Flexible cycle types have been opted for flow, turbulent kinetic energy and specific dissipation rate.

VI. MESH AND MESH INDEPENDENCE

In order to predict turbulence related parameters accurately a high-density mesh is needed in the vicinity of the cylinder. In this research structured mesh with highest possible density was employed close to the cylinder as given in Fig. 2. Inflation with smooth transition in combination with first layer height of less than 3.6×10^{-6} m in accordance with the calculations discussed in section IV.

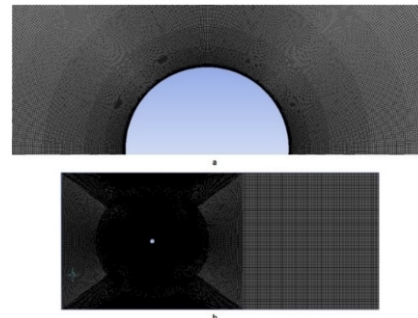


Fig 2 Structured computational mesh with 280584 quadrilateral elements

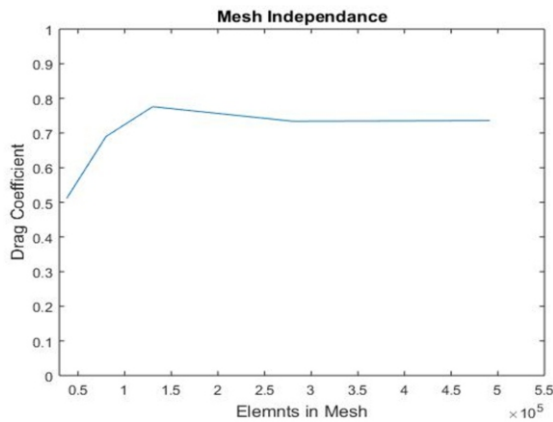


Fig 3 Mesh independence study at $Re\ 1.5 \times 10^6$

The mesh independence details are tabulated in the Table-2 and presented in Figure 3.

Table. 2 Results for checking mesh sensitivity

Sr. No.	Number of Elements	\bar{C}_d
1	37800	0.511
2	80000	0.69
3	130034	0.776
4	280584	0.734
5	491616	0.736

VII. TEMPORAL SENSITIVITY

Time step size is a vital parameter that not only controls accuracy of the results, but also has impact on determining the value of Courant–Friedrichs–Lewy (C-F-L) condition of stability. Time step size can be calculated as per the following formula:[5]

$$\Delta t = \frac{D}{St * U} \quad (10)$$

where,
St is Strouhal Number (St).

C-F-L Number can be calculated based on this Δt as per the following formula:

$$CFL = U \frac{\Delta t}{\Delta x} \quad (11)$$

where,
 Δx represents grid resolution.

Implicit schemes are unconditionally stable as per linear theory of stability, because of this, higher CFL value for implicit schemes are recommended based on the complexity of the problem. CFL number employed in this research was in the range of 13-16 slightly higher than the values attained by the Equation (11).

Table. 3 Results of time step independence study

Sr. No.	Time Step Size	\bar{C}_d
1	0.0002	0.61
2	0.0005	0.71
3	0.0009	0.68

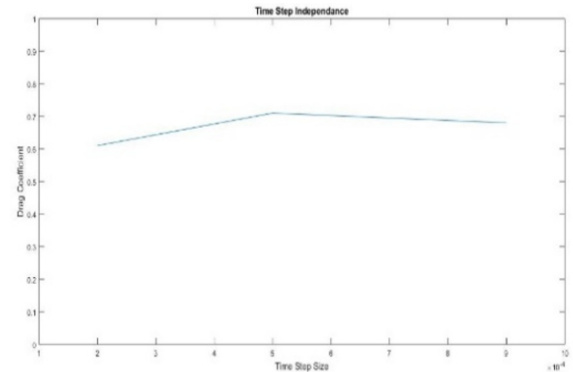


Fig 4 Time Step Independence at $Re\ 1.5 \times 10^6$

Table 3 and Fig. 4 present time independence of the simulations at $Re\ 1.5 \times 10^6$.

VIII. RESULTS

C_d , St and angle of separation (φ) for experimental and numerical data reported in literature along with current simulations is summarized in Table-4. St and φ predicted by 2D URANS model of SST $k-\omega$ are in good agreement with those of Shaghfian et. al. C_d is closer to the experimental results of Roshko and Achenbach in contrast to Shaghfian et. al. and Ishak Yuce et. al.[10-12, 16]

Table. 4 Numerical and experimental values of C_d , St and φ in UTR

Model	Re ($\times 10^6$)	C_d	St #	φ ($^\circ$)
Current				
2 D URANS SST $k-\omega$	1.5	0.61	0.29	110
2 D URANS SST $k-\omega$	2	0.64	0.29	106
2 D URANS SST $k-\omega$	2.7	0.73	0.29	106
2 D URANS SST $k-\omega$	3	0.74	0.28	104.5
2 D URANS SST $k-\omega$	3.6	0.844	0.27	-

Experimental				
Roshko[11]	1-3.5	0.3-0.7	0.27	-
Ashenbach[10]	0.5-5	0.6-0.76	0.5-0.3	115-120
Numerical				
2D SST k-ω[16]	1.5	0.51	-	-
	2	0.552	-	-
	4	0.47	-	-
2D k-ϵ (Linear-CLS) [12]	3.6	0.64	0.29	104
2D k-ϵ (Non-Linear-CLS) [12]	3.6	0.67	0.31	108

Co-efficient of pressure (C_p) with respect to trailing edge of cylinder at $Re\ 1.5 \times 10^6$, 2×10^6 , 3×10^6 and 3.6×10^6 are presented in Fig. 5. The magnitude of peak values of C_p increase for $Re\ 1.5 \times 10^6$, 2×10^6 , 3×10^6 , however, at $Re\ 3.6 \times 10^6$ magnitude of C_p decreases. The trend agrees with experimental trend reported by Achenbach both in quantity and quality. [10, 14] From the graph it can also be noticed that the peak value of C_p first shifts upstream with $Re\ 1.5 \times 10^6$, 2×10^6 , 3×10^6 and then it shifts downstream at $Re\ 3.6 \times 10^6$ in agreement with the trend of C_d and angle of separation.

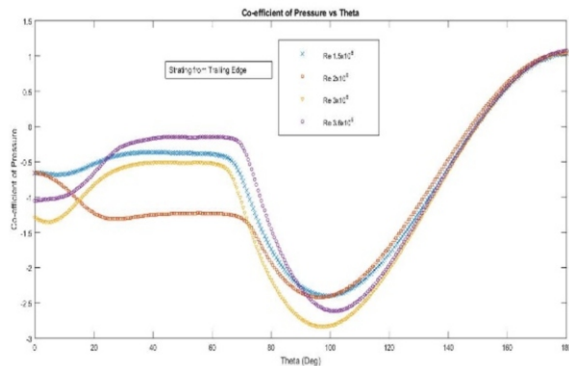


Fig 5 Pressure Co-efficient for 2D URANS SST k- ω at $Re\ 1.5 \times 10^6$, 2×10^6 , 3×10^6 and 3.6×10^6
 Velocity contours of the numerical simulations depict attached separation bubble on both sides of the cylinder in Fig. 6. These attached separation bubbles on both sides of the cylinder result in P-type vortices shedding from the cylinder in UTR. Fig. 6 reiterates the capability of SST-k ω to successfully capture separation of flow.

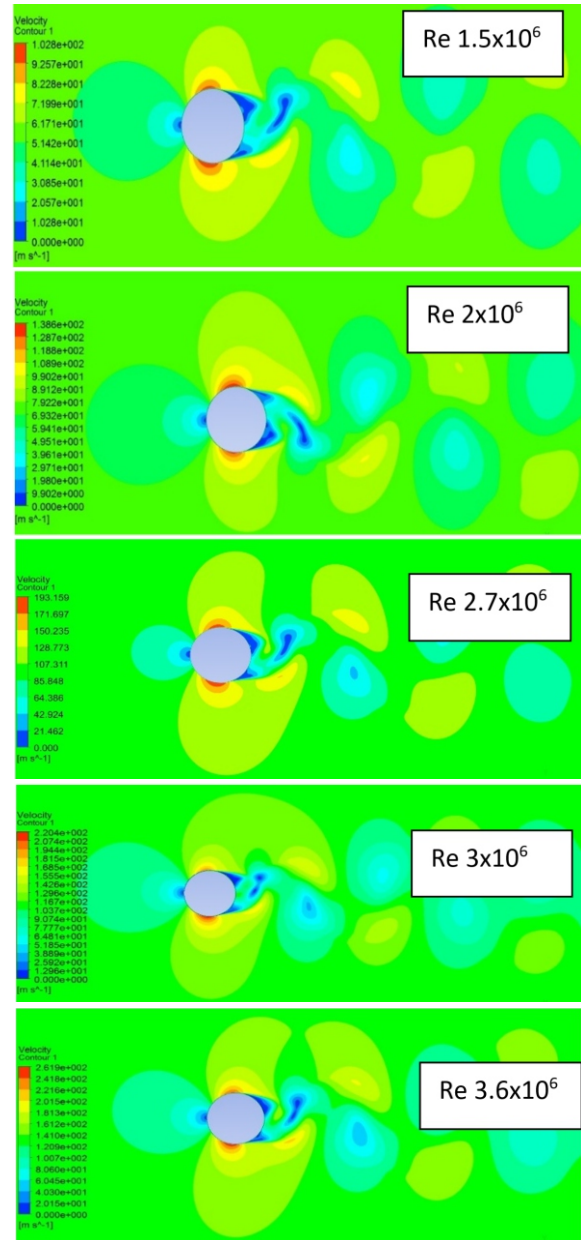


Fig. 6 Velocity contours showing attached P-type separation bubble at $Re\ 1.5 \times 10^6$, 2×10^6 , 2.7×10^6 , 3×10^6 and 3.6×10^6

It has been reported in literature that in UTR turbulence of boundary layer persists on one side of the cylinder. [16] Fig. 7 presents velocity streamlines which show that the turbulence in UTR happens on one side of the cylinder.

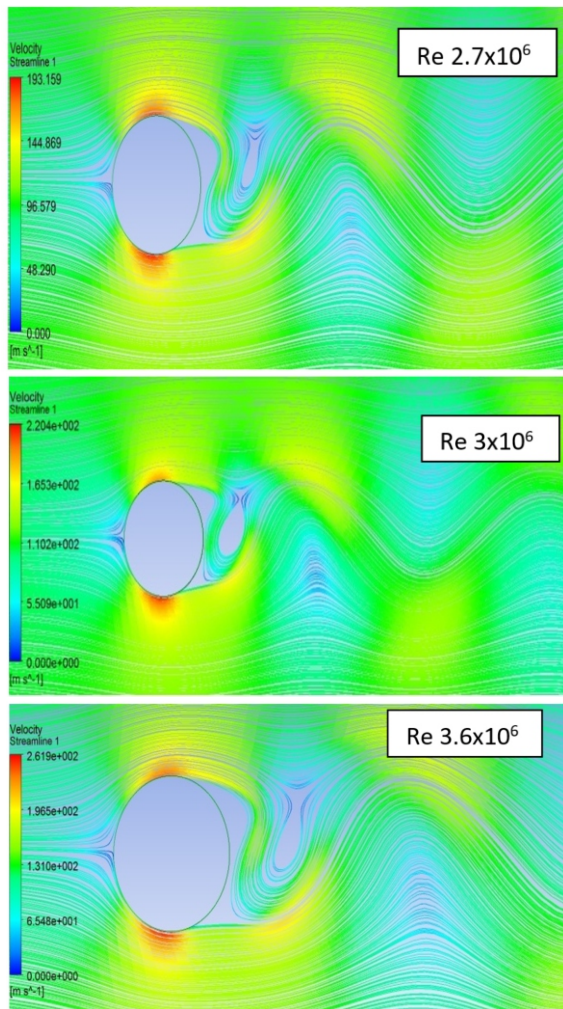


Fig. 7 Streamlines depicting turbulence one side of cylinder at $Re\ 2.7 \times 10^6$, 3×10^6 and 3.6×10^6

It can further be noticed that with increasing Re , velocity gradients across the streamlines just behind the cylinder increase, hinting the onset of TCR beyond $Re\ 3.6 \times 10^6$.

St and Re graph for 2D URANS SST $k-\omega$ model and

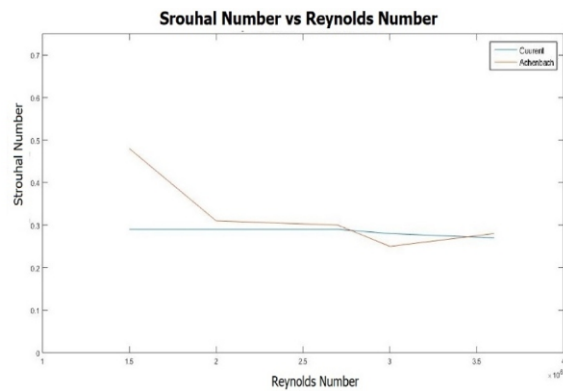


Fig. 8 Reynolds Number vs Strouhal Number in UTR

Achenbach at $Re\ 1.5 \times 10^6$, 2×10^6 , 2.7×10^6 , 3×10^6 and 3.6×10^6 is presented in Fig. 8. The model predicts almost a uniform unchanging St values for across UTR, in contrast to the experimental results of Achenbach [10] that shows a rapid drop of St from $Re\ 1.5 \times 10^6$ to 2×10^6 .

Cd and Re values are plotted in Fig. 9 for 2D URANS SST $k-\omega$ model and Achenbach at $Re\ 1.5 \times 10^6$, 2×10^6 , 3×10^6 and 3.6×10^6 . Available values of numerical investigations of Shaghfian [12] and Ishak Yuce [16] are also plotted. It is evident that current investigation captures the trend of Cd both in quality and quantity.

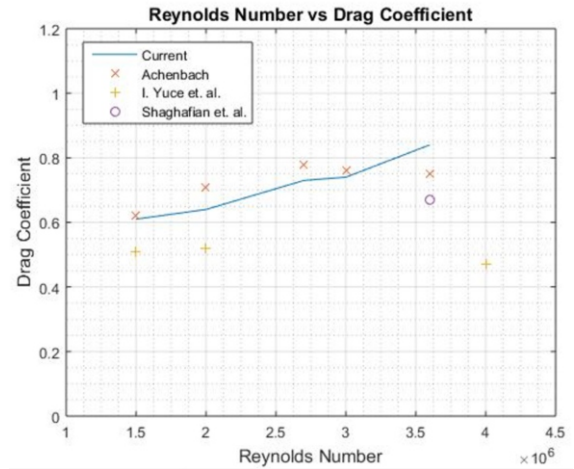


Fig. 9 Reynolds Number vs Coefficient of Drag in UTR

XI. DISCUSSION

The results of few numerical investigations for UTR reported in literature so far have discrepancies in quality and/or quantity in comparison to the experimental investigations. The reasons for these discrepancies are:

- i. these investigations are generic in their approach i.e., they explore all flow regimes of a cylinder at a time,
- ii. these investigations use RANS/URANS model of $k-\epsilon$ and its variants, and
- iii. the investigations employ same numerical approach in terms of grid resolution and numerical schemes across all the regimes.

The flow around cylinder exhibits a changing behavior from laminar to turbulent with increasing Re and there is no single turbulent model that can handle all these the regimes. For example SST can predict onset of separation, while, $k-\omega$ model has a specialty of handling near wall turbulence based on its advanced wall function. [17] Grid resolution near wall has been known to be very crucial and it is expected from researchers to have few layers of computational cells inside the boundary layer. As the flow regime changes, the height of the boundary layer changes, consequently changing the requirement of grid resolution in the

boundary layer region. This requirement of changing the grid resolution seems to be ignored by the some of the researchers as they go across the regimes at a time.

X. CONCLUSION

Flow in UTR around a smooth circular cylinder has been investigated at Re 1.5×10^6 , 2×10^6 , 2.7×10^6 , 3×10^6 and 3.6×10^6 by using 2D URANS model of SST $k-\omega$ in this research. The model has been successful at predicting attached separation bubbles on both sides of the cylinder and hence associated P-type vortex shedding, a characteristic of the regime. The model is handy at predicting the turbulence and separation of flow from the cylinder. The 2D URANS model of SST $k-\omega$ has predicted C_d in close agreement with Achenbach both in quantity and quality across UTR. It is concluded from the results of the current investigation that 2D URANS model of SST $k-\omega$ can be employed for accurate engineering design purposes at $1.5 \times 10^6 \leq Re < 3.6 \times 10^6$.

REFERENCES

- [1] H. Jiang, "Separation angle for flow past a circular cylinder in the subcritical regime," *Physics of Fluids*, vol. 32, p. 014106, 2020.
- [2] M. Aswathy and S. Sarkar, "Nonlinear Dynamics of Circular Cylinders Undergoing Vortex Induced," *Dynamics and Control of Energy Systems*, p. 195, 2019.
- [3] A. Desai, S. Mittal, and S. Mittal, "Experimental investigation of vortex shedding past a circular cylinder in the high subcritical regime," *Physics of Fluids*, vol. 32, p. 014105, 2020.
- [4] C. Zhang, S. Moreau, and M. Sanjosé, "Turbulent flow and noise sources on a circular cylinder in the critical regime," *AIP Advances*, vol. 9, p. 085009, 2019.
- [5] J. D. Anderson and J. Wendt, *Computational fluid dynamics* vol. 206: Springer, 1995.
- [6] H. Ye and D. Wan, "Benchmark computations for flows around a stationary cylinder with high Reynolds numbers by RANS-overset grid approach," *Applied Ocean Research*, vol. 65, pp. 315-326, 2017.
- [7] Y. Cao, T. Tamura, and H. Kawai, "Spanwise resolution requirements for the simulation of high-Reynolds-number flows past a square cylinder," *Computers & Fluids*, vol. 196, p. 104320, 2020.
- [8] S. Kim, P. A. Wilson, and Z.-M. Chen, "Large-eddy simulation of the turbulent near wake behind a circular cylinder: Reynolds number effect," *Applied Ocean Research*, vol. 49, pp. 1-8, 2015.
- [9] S. M. Yeon, J. Yang, and F. Stern, "Large-eddy simulation of the flow past a circular cylinder at sub-to super-critical Reynolds numbers," *Applied Ocean Research*, vol. 59, pp. 663-675, 2016.
- [10] E. Achenbach, "Distribution of local pressure and skin friction around a circular cylinder in cross-flow up to $Re = 5 \times 10^6$," *Journal of Fluid Mechanics*, vol. 34, pp. 625-639, 1968.
- [11] A. Roshko, "Experiments on the flow past a circular cylinder at very high Reynolds number," *Journal of fluid mechanics*, vol. 10, pp. 345-356, 1961.
- [12] M. Saghafian, P. Stansby, M. Saidi, and D. D. Apsley, "Simulation of turbulent flows around a circular cylinder using nonlinear eddy-viscosity modelling: steady and oscillatory ambient flows," *Journal of fluids and structures*, vol. 17, pp. 1213-1236, 2003.
- [13] A. Benim, M. Cagan, A. Nahavandi, and E. Pasqualotto, "RANS predictions of turbulent flow past a circular cylinder over the critical regime," in *Proceedings of the 5th IASME/WSEAS international Conference on Fluid Mechanics and Aerodynamics*, 2007, pp. 232-237.
- [14] M. C. Ong, T. Utnes, L. E. Holmedal, D. Myrhaug, and B. Pettersen, "Numerical simulation of flow around a smooth circular cylinder at very high Reynolds numbers," *Marine Structures*, vol. 22, pp. 142-153, 2009.
- [15] B. Rajani, A. Kandasamy, and S. Majumdar, "On the reliability of eddy viscosity based turbulence models in predicting turbulent flow past a circular cylinder using URANS approach," 2012.
- [16] M. I. Yuce and D. A. Kareem, "A numerical analysis of fluid flow around circular and square cylinders," *Journal-American Water Works Association*, vol. 108, pp. E546-E554, 2016.
- [17] H. Versteeg and W. Malalasekera, "An introduction to computational fluid dynamics," *Finite Volume Method, Essex, Longman Scientific & Technical*, 1995.
- [18] H. Schlichting and K. Gersten, *Boundary-layer theory*: Springer, 2016.